# Robustness and Performance Trade-Offs in Control Design for Flexible Structures

Gary J. Balas, *Member, IEEE*, and John C. Doyle

***Abstract*—Linear control design models for flexible structures are only an approximation to the "real" structural system. There are always modeling errors or uncertainty present. Descriptions of these uncertainties determine the trade-off between achievable performance and robustness of the control design. In this paper it is shown that a controller synthesized for a plant model which is not described accurately by the nominal and uncertainty models may be unstable or exhibit poor performance when implemented on the actual system. In contrast, accurate structured uncertainty descriptions lead to controllers which achieve high performance when implemented on the experimental facility. It is also shown that similar performance, theoretically and experimentally, is obtained for a surprisingly wide range of uncertain levels in the design model. This suggests that while it is important to have reasonable structured uncertainty models, it may not always be necessary to pin down precise levels (i.e., weights) of uncertainty. Experimental results are presented which substantiate these conclusions.**

## I. Introduction

ADVANCES in the control of large flexible structures are necessary to meet pointing and shape accuracy requirements of future space missions. These structures will have numerous lightly damped, densely packed flexible body modes. Due to their size and complexity, ground testing in earth's environment will lead to system models that are inaccurate for operation in a zero-$g$ environment. Even with on-orbit identification of the structure, discrepancies between mathematical models and the "real" structure will still exist, though to a lesser extent. Therefore, control design methods must account for model inaccuracies or uncertainties. Such methods should optimize the controller robustness and performance characteristics based on the accuracy of the design model. Hence, accurate accounting and characterization of variations between "real" flexible structures and their mathematical models is essential [1]-[3].

This paper addresses incorporation of model mismatch between the physical system and its mathematical descriptions into the control design process using the structured singular value ($\mu$) framework. Control design models based on a nominal structural model, uncertainty descriptions, and additive noise models are developed. They define a family or set of uncertain plant models in which the physical system is assumed to reside. $\mu$-synthesis, via $D - K$ iteration, is used to generate vibration suppression controllers for the Caltech experimental flexible structure. Vibration suppression for flexible structures is an active area of research and a complete summary of this work will not be attempted in this paper [4]-[7]. Since the physical structure is assumed to lie inside the model set, measures of robustness and performance characteristics of the controllers are evaluated and predicted when implemented on the flexible structure experiment.

Controllers are synthesized for the experiment with varying levels of uncertainty in the design model. In this paper it is shown that a controller synthesized for a plant model which is not described accurately by the nominal and uncertainty models may be unstable or exhibit poor performance when implemented on the actual system. In contrast, accurate structured uncertainty descriptions lead to controllers which achieve high performance when implemented on the experimental facility. It is also shown that similar performance, theoretically and experimentally, is obtained for a wide range of uncertain levels in the design model. This suggests that while it is important to have reasonable structured uncertainty models, it may not always be necessary to pin down precise levels (i.e., weights) of the uncertainty.

The following sections describe the Caltech flexible structure experiment and provide a brief overview of the structured singular value ($\mu$) framework. Trade-offs associated with uncertainty modeling of flexible structures are discussed. These trade-offs are incorporated into the problem formulation in the form of robustness and performance measures. A series of controllers are synthesized based on different uncertainty descriptions for the Caltech flexible structure. Experimental results of the implementation of the control designs are presented and the results summarized.

## II. Caltech Experimental Flexible Structure

The Caltech experimental flexible structure is designed to include a number of attributes associated with large flexible space structures [1], [2], [8]. These include lightly damped, closely spaced modes, collocated and noncollocated sensors and actuators, and numerous modes in the controller crossover region. The experimental structure, Fig. 1, consists of two bays, three columns, three noncollocated sensors, and actuators for control and an air actuator for disturbance. The entire structure is suspended from a mounting structure fixed to the ceiling to alleviate the problem of column buckling. The three

Manuscript received September 9, 1993. Recommended by Associate Editor, E. Collins. This work was supported in part NASA Langley Control/Structure Interaction Group Grant NAG-1-821, NSF Grant ECS-9110254, the University of Minnesota McKnight Land-Grant Professorship Program, and the University of Minnesota Graduate Research Fellowship Program.

G. J. Balas is with the Department of Aerospace Engineering and Mechanics, University of Minnesota, Minneapolis, MN 55455 USA.

J. C. Doyle is with the Department of Electrical Engineering, California Institute of Technology, Pasadena, CA 91125 USA.

IEEE Log Number 9406373.

1063-6536/94$04.00 © 1994 IEEE

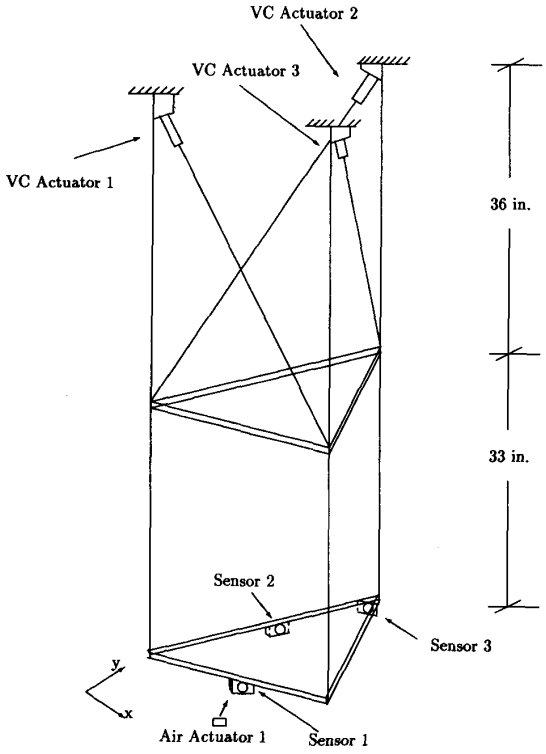


Fig. 1. Phase I Caltech flexible structure.

voice coil actuators are attached to the mounting structure and act along the diagonals of the first story. The air actuator is mounted next to the structure and blows directly on sensor 1. The three sensors are accelerometers that are located on the second bay platform.

### A. Voice Coil Actuators

The voice coil actuators, fabricated by Northern Magnetics Inc., are similar to typical loudspeakers outputting a force proportional to the input voltage. The actuators are mounted in line with the column diagonals and are rated at $\pm 1.36$ kg (3 lbs) of force at $\pm 5$ volts with a 60 Hz bandwidth.

### B. Air Actuators

An air actuator is used as input disturbance to the second-story platform. It blows a stream of air directly on accelerometer 1. The actuator consists of compressed air, which is pulsed on and off by a solenoid. A model of air actuator is difficult to formulate because no accurate measurement of the orifice diameter, air pressure in the line, or force being exerted at the sensor is available. Hence a model of the actuators is experimentally derived by inputting a sinusoidal frequency sweep between 1 and 6 Hz in to the solenoid and measuring the response of the structure. A first-order, 3 Hz bandwidth input disturbance model is developed.

### C. Accelerometers

Sunstrand QA-1400 accelerometers are the sensors. These are mounted on the second-story platform, located along the $x$-axis, $y$-axis, and at 45 degrees to both axes. The accelerometers have a flat frequency response between zero and 200 Hz and are extremely sensitive. The sensor noise is rated at 0.05% of the output at 0–10 Hz and 2% at 10–100 Hz. The accelerometers are scaled for accelerations of .016 g per volt to provide a maximum $\pm 5$ volts output at peak accelerations of the input disturbance. Their output is conditioned by a 100 Hz, fourth order Butterworth filter prior to input into the Masscomp analog/digital (A/D) converter.

TABLE I
DAMPING RATIOS AND NATURAL FREQUENCIES OF THE CALTECH STRUCTURE

| Mode | Experimental Natural Frequency (Hz) | Damping Ratio | Mode Type |
|---|---|---|---|
| 1 | 1.17 | 1.8 % | 1*st* X bending |
| 2 | 1.19 | 1.8 % | 1*st* Y bending |
| 3 | 2.26 | 1.0 % | 1*st* torsional |
| 4 | 2.66 | 1.6 % | 2*nd* X bending |
| 5 | 2.75 | 1.8 % | 2*nd* Y bending |
| 6 | 4.43 | 0.9 % | 2*nd* torsional |

### D. System Identification of Experimental Transfer Functions

System identification techniques are used to develop a six-mode multivariable model of the structure for control design [1], [2]. First, Chebyshev polynomials are employed to fit the experimental data with four single-input/multi-output (SIMO) transfer function models. The curve fitting technique uses a maximum magnitude error criteria to fit the data. This is similar to an $\mathcal{H}_\infty$ norm bound on the error. Table I contains a list of natural frequencies and damping values derived from experimental data.

Combining these SIMO models leads to a multivariable model with 12 modes versus six in the original finite element model in the frequency range of interest. An ad hoc model reduction technique, based on *a priori* knowledge of the structural system and singular value decomposition methods, is used to develop a multivariable system description with six modes. Variations between the identified multivariable model and the experimental data are accounted for by uncertainty descriptions. The identified multivariable model is used as the baseline nominal plant description in the control problem formulation. A more detailed description of the identification method can be found in reference [8].

### E. Real-Time Control Implementation

The controllers are implemented on the Caltech flexible structure via a 5400 Masscomp computer. The real-time control program implements a 60th order, three-input/three-output controller at 200 Hz and generates disturbance commands for the air actuator. The system has a 12 bit A/D converter with a range of $\pm 5$ volts, .00244 volts per bit, and a 12 bit D/A converter with a range of $\pm 5$ volts. The noise associated with

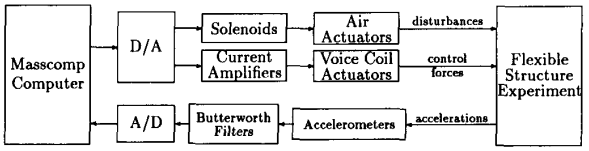


Fig. 2. Block diagram of experimental setup.

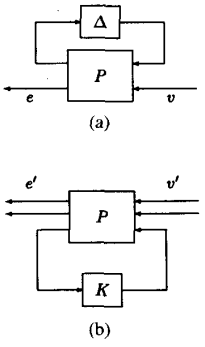


Fig. 3. Standard (a) control analysis and (b) synthesis block diagrams.

the computer is $\pm 1$ lsb (least significant bit). A block diagram of the experimental setup is shown in Fig. 2.

## III. Structured Singular Value ($\mu$) Framework

Linear fractional transformations (LFT's) form the basis of the structured singular value ($\mu$) framework. Fig. 3 shows the standard control analysis and synthesis block diagrams. The $\Delta$ block corresponds to structured perturbations or uncertainties and $K$ corresponds to the controller. Any linear interconnection of inputs, outputs, commands, perturbations, and controller can be rearranged to match these diagrams. The $\mu$ framework allows the incorporation of knowledge of the modeling errors and performance objectives, both in terms of frequency response data, into the control analysis and design problem.

LFT's and $\mu$ provide a common framework in which to analyze and synthesize for robustness and performance requirements. $\mu$ is used to analyze linear fractional transformations when the $\Delta$ block has structure. $\mu$ is defined for a general matrix $M \in C^{n\times n}$ as

$$\mu(M) := (\min\{\overline{\sigma}(\Delta)\colon \Delta \in \boldsymbol{\Delta},\ \det(I + M\Delta) = 0\})^{-1}$$

unless no $\Delta \in \boldsymbol{\Delta}$ makes $(I+M\Delta)$ singular, then $\mu(M) = 0$. In the definition of $\mu(M)$ there is an underlying structure $\Delta \in \boldsymbol{\Delta}$ where $\boldsymbol{\Delta}$ is a prescribed set of block diagonal matrices defined as

$$\boldsymbol{\Delta} = \{\mathrm{diag}(\delta_1 I_{r_1}, \cdots, \delta_s I_{r_s}, \Delta_1, \cdots, \Delta_f)\colon \delta_i \in C, \Delta_j \in C^{m_j \times m_j}\}.$$

$\delta_i$ represents a repeated scalar block and $\Delta_i$ represents a full matrix block. The unit ball, norm bounded set $\mathbf{B}\boldsymbol{\Delta}$, is defined as $\mathbf{B}\boldsymbol{\Delta} = \{\Delta \in \boldsymbol{\Delta}\colon \overline{\sigma}(\Delta) \le 1\}$. The sets $\mathbf{Q}$ and $\mathbf{D}$ leave $\Delta$ invariant in the sense that if $\Delta \in \boldsymbol{\Delta}$, $Q \in \mathbf{Q}$ and $D \in \mathbf{D}$ then $\overline{\sigma}(\Delta Q) = \overline{\sigma}(Q\Delta)$ and $D\Delta D^{-1} = \Delta$. Since $\mu$ itself is difficult to compute, the sets $\mathbf{Q}$ and $\mathbf{D}$ can be used to obtain bounds for $\mu$

$$\mathbf{Q} = \{Q \in \boldsymbol{\Delta}\colon Q^*Q = I_n\}$$
$$\mathbf{D} = \{\mathrm{diag}(D_{r_1}, \cdots, D_{r_s}, d_1 I_{m_1}, \cdots, d_f I_{m_f})\colon D_i = D_i^* > 0, d_i \in R_+\}$$
$$\sup_{Q\in\mathbf{Q}} \rho(MQ) \le \mu(M) \le \inf_{D\in\mathbf{D}} \overline{\sigma}(DMD^{-1})$$

where $\rho$ denotes the spectral radius and $\overline{\sigma}$ denotes the maximum singular value. A more complete background on $\mu$ is found in references [9]-[12].

The control design approach is to minimize the $\mu$ upper bound since synthesizing a controller to minimize $\mu$ directly is too difficult. $D-K$ iteration, a $\mu$-synthesis methodology, is used to design controllers to achieve the desired robust performance objectives by integrating $\mathcal{H}_\infty$ control design with $\mu$ analysis [13], [15], [16], [12]. Since the upper bound for $\mu$ may be obtained by scaling and applying the $\|\cdot\|_\infty$, $D-K$ iteration approximates $\mu$-synthesis by finding a stabilizing controller $K$ and a scaling matrix $D$ such that the quantity $\|DF_l(P,K)D^{-1}\|_\infty$ is minimized. $D-K$ iteration alternately minimizes the above expression with respect to $K$ or $D$ holding the other matrix constant.

First consider holding $\hat{D}(s)$ fixed. Given a stable, minimum phase, real-rational $\hat{D}(s)$, define $P_D$ as

$$P_D = \begin{bmatrix} D & 0 \\ 0 & I_{n\mathrm{meas}} \end{bmatrix} P \begin{bmatrix} D^{-1} & 0 \\ 0 & I_{n\mathrm{cntl}} \end{bmatrix}.$$

The following results trivially hold: $K$ stabilizes $P_D$ if and only if $K$ stabilizes $P$; $F_l(P_D, K) = DF_l(P,K)D^{-1}$ where $P_D$ is a real-rational transfer function matrix. Hence, solving the optimization $\min_{\substack{K \\ \mathrm{stabilizing}}} \|\hat{D}F_l(P,K)\hat{D}^{-1}\|_\infty$ is the same as $\min_{\substack{K \\ \mathrm{stabilizing}}} \|F_l(P_D,K)\|_\infty$. The last equation is an $\mathcal{H}_\infty$ optimization control problem. The solution to the $\mathcal{H}_\infty$ problem is well known and consists of solving algebraic Riccati equations in terms of the state-space system $P_D$ [13].

Given a stabilizing controller, $K(s)$, solve the following minimization corresponding to the upper bound for $\mu$

$$\min_{D_\omega \in \mathbf{D}} \overline{\sigma}\left[D_\omega F_l(P,K)(j\omega)D_\omega^{-1}\right].$$

This minimization is done over the {real, positive} $D_\omega$ from the set $\mathbf{D}$. Note that the addition of phase to each $d_i$ does not affect the value of $\overline{\sigma}\left[D_\omega F_l(P,K)(j\omega)D_\omega^{-1}\right]$ [16]. Hence, each discrete function, $d_i$, of frequency is fit (in magnitude) by a proper, stable, minimum-phase transfer function, $\hat{d}_{R_i}(s)$. Although this iteration scheme is not guaranteed to reach the global optimum, it has been applied with great success to vibration suppression for flexible structures, flight control, and chemical process control problems [3], [12], [14], [15].

## IV. Robustness and Performance Trade-Offs

Selection of uncertainty descriptions plays a major role in the trade-off between robustness and performance requirements in the control design process. A controller design based on an assumed "perfect" model leads to a high performance design on the model, but when implemented on the "real"

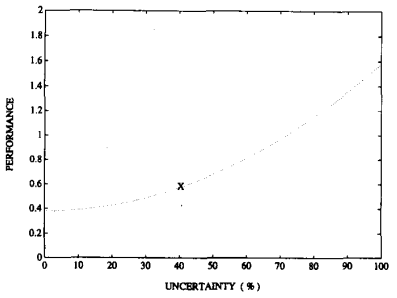


Fig. 4. Control design, $\overline{K}$, for an uncertainty level of 40%.

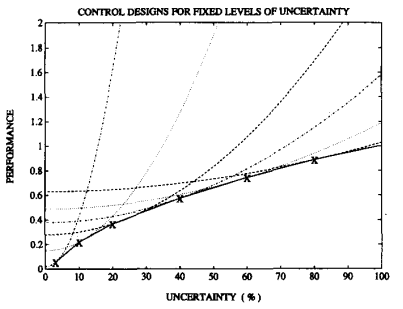


Fig. 5. Six controller for uncertainty levels of 3%, 10%, 20%, 40%, 60%, and 80%.

system it may be destabilizing or exhibit poor performance. This is attributed to the control design methodology optimizing the controller based only on the information provided it, which it assumes is "perfect." Models, though, are only approximations to physical systems. Uncertainty descriptions provide a quantitative measure of variations between mathematical models and the physical system. It is essential that a control design methodology include uncertainty descriptions into the optimization process. A major attribute of $\mu$ is the incorporation of both robustness and performance objectives into a compatible control analysis and design framework.

Uncertainty descriptions and levels are directly related to physical modeling of the problem and need to be developed based on actual system characteristics. For example, choosing a large uncertainty model, unmotivated by physical data, can lead to overly conservative control designs, thereby limiting performance of the control design. A trade-off exists between robustness of the control law and performance objectives in the design process.

To better illustrate this trade-off, consider synthesis of a hypothetical controller for a specific level of uncertainty, $\alpha$, using $\mu$-synthesis techniques. The data used in this example is not real; it is used to illustrate the trade-off between robustness and performance which occurs in real physical systems. For a prescribed level of uncertainty, $\alpha$, we are able to design a controller, $\overline{K}$, which achieves a "worst-case" performance level of $\beta$, corresponding to $\frac{1}{\text{performance_weight}}$. This provides the point "×" on the curve in Fig. 4. A $\beta$ equal to one corresponds to the closed-loop, worst-case performance equaling the open-loop performance, for $\beta < 1$, the closed-loop worst-case performance is better than the open-loop, and for $\beta > 1$ it is worse. Assuming the system to be controlled is described exactly by the set of plants defined by the nominal model and uncertainty descriptions, the level of performance achieved for the worst case input signal affecting the worst case plant model can be formulated as an $\mathcal{H}_\infty$ control problem.

Suppose the initial model set, described by the nominal structural model and uncertainty descriptions, is a conservative representation of the physical structure: That is, extra plants are included in the model set which are not feasible. The controller, $\overline{K}$, designed for this model set will likely achieve better performance when implemented on the physical structure than is anticipated due to the predicted performance level, $\beta$, being based on the worst plant model in the initial model set. If the physical system does not correspond to the worst-case model in the set, the performance level on the closed-loop system will be higher than the theoretically predicted value.

Similarly, if the uncertainty descriptions do not encompass the physical system, the controller may destabilize the system or severely degrade performance. As the difference between the design model and the physical system increases, the performance of the controller, $\overline{K}$, decreases. A graphical representation of this is presented in Fig. 4. The dotted line indicates how the performance, $\beta$, of the control law $\overline{K}$ might vary as a function of the uncertainty level $\alpha$. As an example, the control law $\overline{K}$ is designed for an uncertainty level of 40% and achieves a performance of 0.58. If there is less uncertainty between the "real" system and the model, the controller will exhibit slightly improved performance when implemented. Conversely, if there is more variation between the "real" system and model, the control law performance will degrade.

For the same theoretical example, six controllers, $K_1$ through $K_6$, are designed for 3%, 10%, 20%, 40%, 60%, and 80% uncertainty, each generating a curve similar to Fig. 4. A graph of these curves is shown in Fig. 5. Each "×" in the figure corresponds to the theoretical level of performance the $\mu$-synthesis controller would achieve for a specified level of uncertainty. The solid curve represents the envelope of achievable performance for the control designs based on the nominal model and the uncertainty description. As one would expect, the highest performance is achieved when the nominal model is a perfect representation of the "real" system. Based on these graphs, one can see that accurately describing the physical system with nonconservative sets of plants results in superior performing controllers on the "real" system. This approach can be employed as a means of model validation to verify the consistency of the model and uncertainty descriptions with experimental data.

## V. Vibration Suppression Control Design

The trade-off between robustness and performance via selection of uncertainty descriptions is investigated on the Caltech Phase I flexible structure experiment. Results indicate that an accurate plant (nominal) model and uncertainty descriptions lead to controllers which exhibit superior performance when implemented on the physical system. It is also observed that the location and structure of the uncertainty model in the

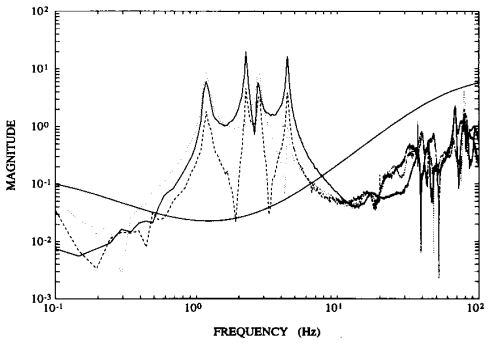


Fig. 6. Frequency response of actuator 2 to sensors and the additive uncertainty weight.

problem formulation has a direct bearing on the performance of multivariable control designs. This is in contrast to single-input/single-output uncertainty models where location in the problem formulation is unimportant.

A series of controllers are designed for the experiment by varying levels of uncertainty and sensor noise weights. One set of controllers is designed using only an additive sensor noise model to account for uncertainty. These controllers destabilize the physical system until the sensor noise level is increased in the problem formulation to the magnitude of the flexible modes response. A second set of controllers is formulated using frequency domain uncertainty descriptions of the variations between the mathematical model and the physical system. These designs make use of an additive uncertainty model to account for high frequency unmodeled dynamics and multiplicative input/output uncertainty to account for actuator/sensor errors and mode shape mismatch. As one traverses from a controller designed with only an additive uncertainty model to one with a significant amount of input/output uncertainty in addition to the additive uncertainty model, the experimental performance level achieved is maximized between the two extremes. These results clearly indicate the trade-off between robustness and performance in control design and the importance of uncertainty descriptions in the control design process.

### A. Control Objective

The control objective is to attenuate vibration of the first six natural frequencies in the Phase I Caltech flexible structure at the three accelerometer locations. The input disturbance is a sine sweep between 1 and 6 Hz commanded to air actuator 1. The output air stream blows directly on the sensor 1. The performance measure is to minimize the maximum frequency response of the first six modes at the sensor locations, as compared with their open-loop response, for a worst case input signal. This specification is formulated as minimizing the $\mathcal{H}_\infty$ norm between the input disturbances and sensor outputs.

### B. Uncertainty Descriptions

Frequency domain uncertainty descriptions are employed to account for the variation between the model and the physical system. An additive uncertainty weight accounts for the low frequency inaccuracies (below 0.8 Hz) and the unmodeled high frequency dynamics (above 8 Hz). The magnitude of the additive uncertainty weight at high frequency is selected to envelope the unmodeled modes of the system. The additive uncertainty weight assures that the high frequency modes are gain stabilized by requiring the control design to satisfy $\|W_{\text{add}}^{-1}KS\|_\infty < 1$, where $K$ is the controller and $S$ is the sensitivity transfer function $(I - P_{\text{nom}}K)^{-1}$. A plot of the frequency response of transfer functions between voice coil actuator 2 and the three sensors along with the additive uncertainty weight is shown in Fig. 6. The additive uncertainty weight is given by

$$W_{\text{add}} = 8\frac{(s+6)(s+12)(s+24)}{(s+.6)(s+400)^2}.$$

Within the controller bandwidth, 1 to 5 Hz, the additive uncertainty takes on its minimum value. This weight is purposely reduced within this frequency range to demonstrate the role additional uncertainty descriptions, i.e., multiplicative input and output uncertainty weights, play in the performance of the controllers. The magnitude of the additive uncertainty weight is selected to insure that all controllers synthesized with this weight would stabilize the structure.

The input and output multiplicative uncertainty are independently varied to gauge their effect on the robustness and performance properties of the controller. These uncertainties are selected to be constant for two reasons. The additive uncertainty weight, $W_{\text{add}}$, dominates the plant model outside of the 0.8 Hz to 8 Hz frequency range. Hence additional multiplicative uncertainty outside the 0.8 Hz to 8 Hz frequency range would have little effect on the plant description. The second reason for selecting a constant multiplicative input and output description is that there is negligible frequency variation in the errors between 1 and 5 Hz.

The multiplicative input uncertainty is used to represent errors in the actuator model and in the mismatch between the experimentally derived transfer function and the model between 0.8 Hz to 8 Hz. Similarly the multiplicative output uncertainty represents errors in the sensor models and output error in the control model. In the control problem formulation, the multiplicative weights are distributed between the inputs and outputs of the uncertainty blocks to provide better initial scaling for the $\mathcal{H}_\infty$ control design algorithms. Despite the number of lightly damped, flexible modes, no numerical problems were encountered using the $\mathcal{H}_\infty$ control design algorithms [12].

### C. Control Problem Formulation

The control problem interconnection structure is shown in Fig. 7. The identified four-input/three-output nominal model of the flexible structure, $P_{\text{nom}}$, is used to model the flexible structure experiment. As stated, the control design must be robust to unmodeled high frequency dynamics and model errors while attenuating the vibrational responses of the first six flexible modes. The additive uncertainty weight is modeled as an unstructured full block uncertainty, $\Delta_1$, around the flexible structure model as seen in Fig. 7.

Multiplicative input and output weights, *actu* and *sensu*, are the parameters varied to examine trade-offs between the

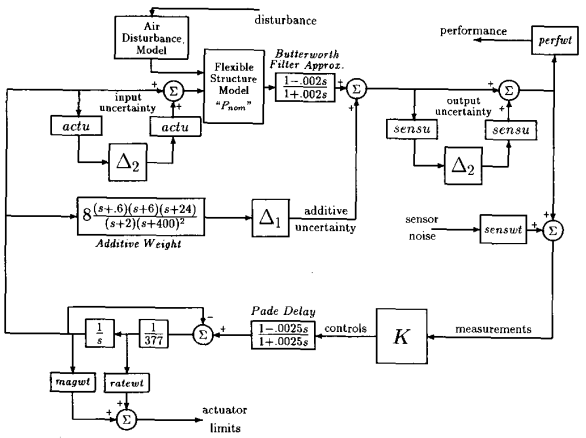


Fig. 7. Block diagram of control problem formulation.

robustness and performance of the control designs. A constant input uncertainty, *actu*, is selected to account for actuator errors and mismatch between the input mode shapes and the experimental data. *actu* is varied from 0 to 0.5, representing a 0 to 25% variation in the uncertainty level associated with the input signals to the flexible structure model. *sensu* represents a constant multiplicative output uncertainty which accounts for sensor errors and output mode shape discrepancies. One set of controllers is formulated with no output multiplicative uncertainty, *sensu*, and the input uncertainty, *actu*, varied. These controllers investigate the effect of input uncertainty descriptions on the performance characteristics of the control designs when implemented on the physical system. Similarly, a set of controllers are synthesized with no input uncertainty, *actu*, and the output multiplicative uncertainty, *sensu*, varied between 0 and 0.5 (0–25% uncertainty) to examine the effect of output uncertainty.

The input and output multiplicative uncertainty models are described by full block unstructured uncertainty. Full block uncertainty descriptions indicate that cross coupling between the input (output) channels is allowed. Representing the uncertainty as scalar blocks would restrict errors to the individual channels (i.e., no cross coupling of uncertainty). During the analysis stage of the control designs, comparisons are made between full and scalar block multiplicative uncertainty models. The three structured scalar uncertainty blocks had $\mu$ values that were 1–3% less than the full block uncertainties. This implies that if the structured uncertainty is a more accurate description of the physical system, it would have 1–3% better robustness margins and exhibit 1–3% better performance than the unstructured uncertainties when implemented. This is a modest difference, hence the unstructured uncertainties are used in the control analysis and design.

The advantage of describing the input uncertainty by a full block as opposed to scalar blocks is two fold: It reduces the number of uncertainty block and accounts for cross feed between channels leading to a more robust control design. The output multiplicative uncertainty is also treated as a full block uncertainty and exhibited similar characteristics to the input uncertainty model.

The performance weight for vibration attenuation is selected as a constant scaling, *perfwt*, on the sensor outputs. The disturbance to acceleration output transfer functions are first scaled to one, then the performance weight, *perfwt*, is used to determine the amount of attenuation of the frequency domain peaks. A constant weighting is sufficient only if one desires the closed-loop performance transfer functions to be flat across frequency with no additional frequency shaping. Since the magnitude of the six flexible modes between 1 and 5 Hz are all on the same order, a constant scaling provides a good weighted performance objective without adding states to the control problem.

The input disturbance enters via air actuator 1 and blows directly on sensor 1. A first-order weight, $\frac{10}{s+10}$, is used to describe the input excitation. Force and rate limits on the voice coil actuators are also included in the control design. The actuator force limit is included by scaling, *magwt*, its output to one when the force is at $\pm 3$ lbs. This scaling needs to be consistent with a unit input level of disturbance. Similarly, the 60 Hz rate limit is scaled with *ratewt*. The sensor noise level for the accelerometers is included as a performance limitation. The weighting, *senswt*, is selected to be $2 \times 10^{-3}$ representing an accelerometer signal to noise ratio of 250. These performance specifications are accounted for in the $\mu$-framework by a full block unstructured uncertainty, resulting in a $\mathcal{H}_\infty$ norm measure. All performance requirements are satisfied when the $\mathcal{H}_\infty$ norm of the performance block is less than one.

The accelerometers are filtered by 100 Hz, fourth-order Butterworth filters before being input into the A/D converter. One can account for these filters with accurate fourth-order models in each channel, but this would entail an additional 12 states in the problem formulation. A first-order approximation of the filters ($\frac{1-.002s}{1+.002s}$) is used instead, resulting in the addition of three states. This approximation matches the magnitude and phase of the fourth-order Butterworth filters well up to 40 Hz. This is far above the controller bandwidth of 5 Hz. Any error induced by this approximation is accounted for by the additive uncertainty weights. A first-order Padé approximation, ($\frac{1-.0025s}{1+.0025s}$), is included to model the 5 ms sample time delay associated with the real time control computer. The complete block diagram is shown in Fig. 7.

The block diagram is reformulated into the LFT general framework to design control laws using the $\mu$-synthesis methodology. A diagram of the LFT is shown in Fig. 8. The dimensions of the $\Delta$ blocks are: $3 \times 3$ for $\Delta_1$, $3 \times 3$ for $\Delta_2$, and $6 \times 4$ for $\Delta_3$. $\Delta_1$ is associated with the additive uncertainty, $\Delta_2$ with the multiplicative input (output) uncertainty, and $\Delta_3$ is the performance block. All the $\Delta_i$ blocks are full blocks. Either input or output multiplicative uncertainty is included in the control problem formulation. In this set of designs, input and output uncertainty are not included simultaneously.

### D. Control Designs: Sensor Noise Only

Six controllers are synthesized based on the block diagram in Fig. 7 with no additive or multiplicative input/output uncertainty. The sensor noise weight, *senswt*, is varied between

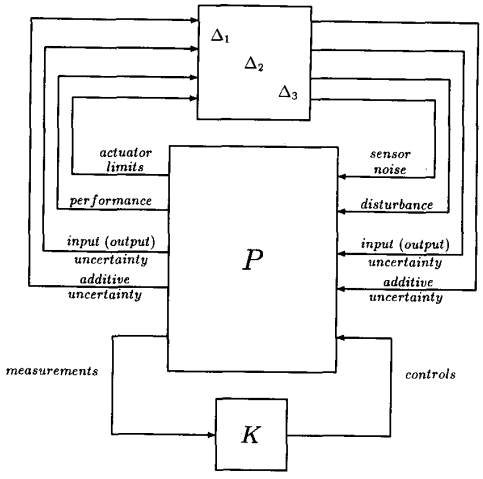


Fig. 8. Linear fractional representation of control problem.

TABLE II
PARAMETERS FOR CONTROL DESIGN WITH SENSOR NOISE

| Controller | Controller Order | *senswt* | *perfwt* | $\mu$ | Predicted Performance | Experimental Performance |
|---|---|---|---|---|---|---|
| $K1sn$ | 32 | $4 \times 10^{-3}$ | 15.00 | 0.99 | .067 | Unstable |
| $K2sn$ | 28 | $4 \times 10^{-2}$ | 14.00 | 0.98 | .071 | Unstable |
| $K3sn$ | 26 | $4 \times 10^{-1}$ | 8.00 | 1.00 | .125 | Unstable |
| $K4sn$ | 30 | $9 \times 10^{-1}$ | 4.75 | 1.00 | .211 | Unstable |
| $K5sn$ | 30 | 1.15 | 4.75 | 1.00 | .253 | Unstable |
| $K6sn$ | 32 | 2.30 | 2.12 | 0.99 | .472 | 0.87 |

$4 \times 10^{-3}$ and 2.3 to account for uncertainty and provide robustness in the control designs. Table II contains a list of the control law parameters used in the design and the results of implementation on the flexible structure experiment. Each control design is synthesized to achieve a robust performance $\mu$ value of 1.

Controllers $K1$sn through $K5$sn destabilize the experimental structure when they were implemented due to the excessive gain at high frequency. Increasing the level of the sensor noise to the magnitude of the flexible mode peaks, $K6$sn, leads to a reduction in the controller gain at low and high frequency. This stabilizes the system, and, in turn reduces the performance of the controllers. Controllers $K1$sn through $K6$sn were stable and achieved their predicted performance in simulations using the nominal model.

This is an extreme example of the shortcomings associated with designing control laws based solely on additive noise models to account for model errors. It illustrates, though, the need to provide information in the model formulation as to the fidelity of the model across a range of frequencies. The structural model is sufficiently accurate between 1 and 5 Hz such that by accounting for the unmodeled dynamics with an additive uncertainty model a controller can be synthesized which stabilizes the system and performs well when implemented. Development of improved uncertainty models can further increase controller performance.

TABLE III
PARAMETERS FOR CONTROL DESIGN WITH INPUT MUTIPLICATIVE UNCERTAINTY

| Controller | Controller Order | Actuator Uncertainty (%) | *perfwt* | Predicted Performance | Experimental Performance | $\mu$ |
|---|---|---|---|---|---|---|
| Open-loop | — | — | — | 1.000 | 1.000 | — |
| $K1am$ | 26 | 0.00 | 13.0 | .077 | 0.087 | 1.02 |
| $K2am$ | 32 | 1.00 | 12.4 | .081 | 0.087 | 1.02 |
| $K3am$ | 32 | 2.25 | 11.0 | .091 | 0.073 | 1.01 |
| $K4am$ | 32 | 4.00 | 10.0 | .100 | 0.082 | 1.02 |
| $K5am$ | 32 | 7.29 | 8.4 | .119 | 0.093 | 1.03 |
| $K6am$ | 32 | 10.00 | 7.1 | .141 | 0.121 | 1.00 |
| $K7am$ | 24 | 14.44 | 5.8 | .172 | 0.142 | 1.08 |
| $K8am$ | 24 | 17.00 | 4.2 | .238 | 0.123 | 1.07 |
| $K9am$ | 24 | 20.25 | 3.9 | .256 | 0.104 | 1.02 |
| $K10am$ | 24 | 25.00 | 2.9 | .345 | 0.161 | 1.02 |

### *E. Control Designs: Input Multiplicative Uncertainty*

A number of controllers are synthesized using additive uncertainty and input multiplicative uncertainty descriptions to account for variations in the model. The output uncertainty, *sensu*, is set to zero in Fig. 7 for this set of designs. Ten controllers are formulated for input multiplicative uncertainty level varying between 0 and 25%. Robustness and performance of the control designs are traded off in the design process, as one is increased the other is decreased. Each design is iterated on until it achieves a $\mu$ value of approximately one. This is done by selecting a desired level of input uncertainty and scaling the performance requirement, *perfwt*, until the control design achieves a $\mu$ value of one.

The value of $\mu$ is highest within the frequency range of the flexible modes to be controlled. Attenuation of these modes is the limiting factor in the controller design, which is often the case in lightly damped, flexible systems. The level of the accelerometer noise was determined from the manufacturers specifications of 0.2% error. The *senswt* is fixed at $2 \times 10^{-3}$ in all designs. The actuator weights, *magwt* and *ratewt*, are selected to correspond to the magnitude and rate limits of the actuators. For these control designs, ımagwt is set to 80 and the *ratewt* is set to 3770. Table III contains the parameters varied in the control designs.

The 10 controllers synthesized are implemented on the flexible structure experiment and compared with the open-loop response. Experimental data is derived from the filtered noise input to air actuator 1 and accelerometer 1, 2, and 3 measurements. The open-loop time and frequency responses of accelerometers 1, 2, and 3 are shown in Fig. 9. The closed-loop experimental time and frequency responses of accelerometers 1, 2, and 3 with controllers $K3$am and $K10$am implemented are shown in Figs. 10 and 11, respectively. The experimental input disturbance to air actuator 1 was a sine sweep from 1 to 5 Hz. Table III contains the experimental data of the closed-loop experiments for each control design.

The original interconnection structure with the plant model and weights shown in Fig. 7 has 32 states. During the $D-K$ iteration procedure, the inputs and outputs associated with the two uncertainties, $\Delta_1$ and $\Delta_2$, are scaled on the left and right with stable, minimum phase proper transfer functions. Second order $D$-scalings are used to scale the first set of uncertainty inputs and outputs and constant $D$-scalings are

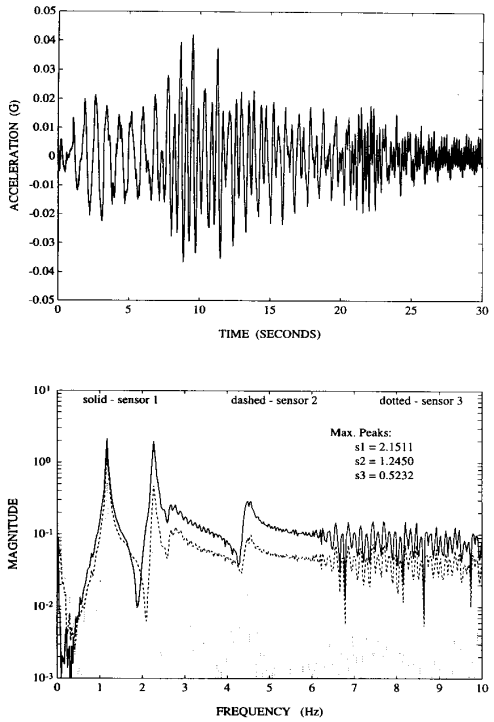


Fig. 9. Open-loop time (sensor 1) and frequency response to input excitation.

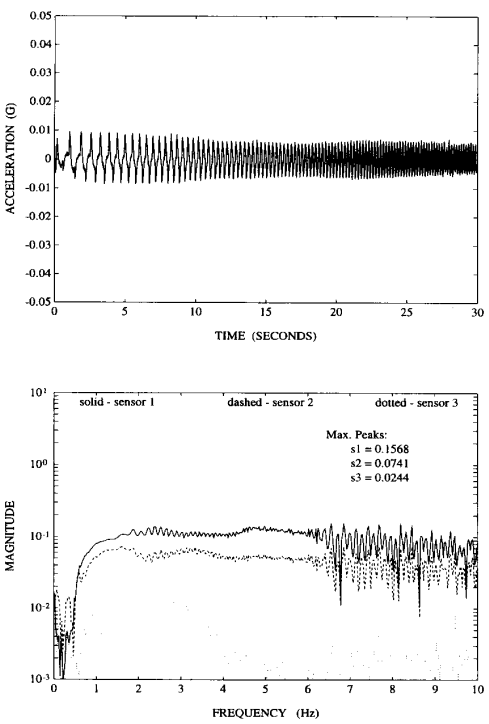


Fig. 10. $K3$am closed-loop time (sensor 1) and frequency response.

used for the second set. The resulting controllers, $K1$am through $K10$am, are 44th order. The balanced realization model reduction technique is used to reduce the state order of

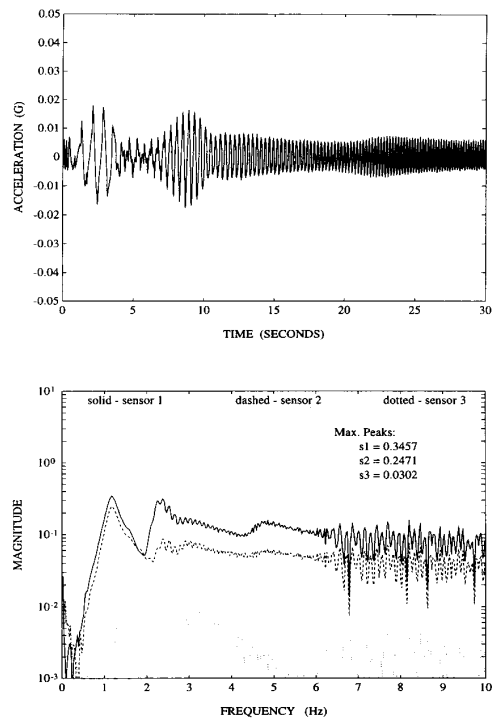


Fig. 11. $K10$am closed-loop time (sensor 1) and frequency response.

the controllers. The order of the controllers is shown in Table III. The controller order was selected such that the lower order controller would have less than a 1% effect on the closed-loop $\mu$ value.

Performance is measured as the maximum closed-loop peak response to the maximum open-loop response since the objective is to attenuate the first six flexible modes. The ratio of the maximum peak of the closed-loop controllers to the open-loop response corresponds to the experimental performance. The best performance, 0.073, representing a reduction of the maximum frequency domain peak by 13.7, is achieved for the controller designed with 2.25% input uncertainty. Controllers designed for higher and lower uncertainty levels than this exhibited reduced levels of performance. $K1$am and $K2$am achieved performance levels less than predicted by the design model, and all other control designs surpass their predicted performance. Fig. 12 is a plot of the designed performance level as a function of input multiplicative uncertainty level. Circles, "$O$," represent the experimental values, and "$X$" represents the model.

One can interpret this graph as one interprets Fig. 5. The set of models described by the problem formulation for designs $K1$am and $K2$am do not encompass the physical system, since the worst case plant description the performance levels are higher than achieved when implemented on the experimental structure. One can infer that the controllers are optimized for an inaccurate model. The set of plant models defined in the control design problems for $K3$am through $K10$am provides a better representation of the physical system than the sensor noise control design model due to the experimental and

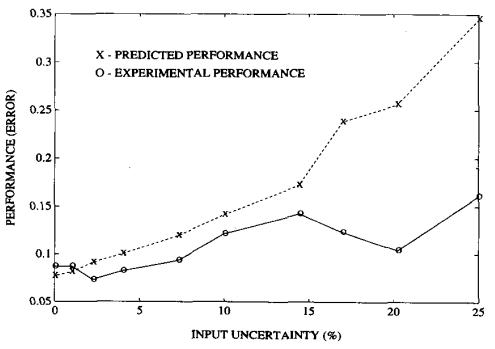


Fig. 12. Predicted versus experimental performance for input uncertainty designs.

performance levels corresponding to the designed performance level. The model sets for control designs $K3$am through $K10$am provide a more accurate description of the physical system for control purposes.

Selecting an appropriate level of uncertainty for this problem description provides the highest level of performance on the structure. Increasing the input uncertainty level results in more conservative controllers which emphasize robustness by reducing the amount of control action. These results indicate that selection of uncertainty descriptions has a direct bearing on the performance and robustness of the controllers.

### F. Control Designs: Output Multiplicative Uncertainty

A set of controllers is synthesized with additive and multiplicative output uncertainty to account for errors in the design model. The problem formulation is based on the interconnection structure in Fig. 7 with the input uncertainty scaling, *actu*, set to zero. Nine control laws are formulated for the output scaling, *sensu*, varying between 0.1 and 0.5. This is analogous to the output multiplicative uncertainty varying between 1% and 25%. Each control law is designed for a specified level of output uncertainty, *sensu*, with the performance weight, *perfwt*, scaled to achieve a $\mu$ value of one.

The set of nine controllers uses the same noise weight, *senswt*, *magwt*, and *ratewt*, as the input uncertainty designs. Table IV contains a list of parameters varied in the output multiplicative uncertainty control designs and experimental results. Each controller is implemented on the structure and an experimental frequency response is generated from the air disturbance input to the three accelerometer outputs. $K1$am is included because it was designed with zero input/output multiplicative uncertainty. During the $D-K$ iteration procedure the inputs and outputs associated with the two uncertainties, $\Delta_1$ and $\Delta_2$, are scaled on the left and right with stable, minimum phase proper transfer functions. As in the input multiplicative uncertainty case, second order $D$-scalings are used to scale the first set of uncertainty inputs and outputs and constant $D$-scalings are used for the second set. The resulting controllers are 44th order. The same criteria and techniques are used to reduce the controller order. The order of the controllers implemented are shown in Table IV.

TABLE IV
PARAMETERS FOR CONTROL DESIGN WITH OUTPUT MUTIPLICATIVE UNCERTAINTY

| Controller | Controller Order | Actuator Uncertainty (%) | *perfwt* | Predicted Performance | Experimental Performance | $\mu$ |
|---|---|---|---|---|---|---|
| Open-loop | — | — | — | 1.000 | 1.000 | — |
| $K1am$ | 26 | 0.00 | 13.0 | .077 | 0.087 | 1.02 |
| $K2sm$ | 24 | 1.00 | 11.60 | .086 | 0.085 | 1.03 |
| $K3sm$ | 24 | 2.25 | 10.95 | .091 | 0.072 | 0.95 |
| $K4sm$ | 24 | 4.00 | 10.40 | .096 | 0.082 | 1.05 |
| $K5sm$ | 24 | 7.29 | 9.70 | .103 | 0.084 | 1.03 |
| $K6sm$ | 24 | 10.00 | 9.10 | .110 | 0.091 | 1.06 |
| $K7sm$ | 24 | 14.44 | 8.80 | .114 | 0.084 | 1.03 |
| $K8sm$ | 24 | 17.00 | 8.40 | .119 | 0.086 | 0.96 |
| $K9sm$ | 22 | 20.25 | 8.10 | .124 | 0.097 | 1.07 |
| $K10sm$ | 22 | 25.00 | 7.75 | .129 | 0.106 | 1.09 |

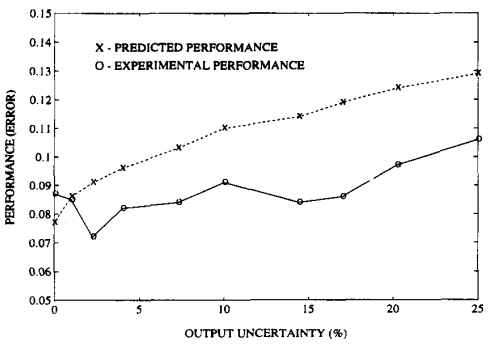


Fig. 13. Predicted versus experimental performance for output uncertainty designs.

Controller $K3$sm achieved the highest level of performance, 0.072. $K1$am had a performance level less than predicted, and all other controllers exceeded their predicted performance. Fig. 13 provides a comparison between the predicted performance of the model, given the designed uncertainty level and the experimental data. Note the consistent trend in the data between the theory and the experiments. As expected, increasing the output uncertainty weight increases the robustness characteristics of the control law at the expense of the performance. The high correlation between the experimental and predicted performance levels indicate that the nominal model with output multiplicative uncertainty provides an excellent model of the experimental flexible structure for the purpose of control. The results in Table IV and Fig. 13 also indicate that it is more important to have some reasonable level (1–17%) of uncertainty and the correct location of the uncertainty rather than the exact amount of uncertainty included in the problem formulation. This has implications in the development of nominal and uncertainty models using system identification techniques from experimental data.

One explanation for why the output multiplicative uncertainty control design model closely parallels experimental results is due to the structural model. The nominal structural model was derived using a single-input/multi-output system identification technique. It is found that the input directions closely match the experimental data. The output directions vary slightly due to method of curve fitting the experimental data. Therefore output multiplicative uncertainty by itself is

likely to better characterize the modeling error from fitting the three sensor measurements from a single input.

## VI. Summary

An accurate representation of the physical system by a nominal model and an uncertainty description provides an excellent design model for use in the $\mu$-synthesis techniques. The addition of uncertainty models is required because the inclusion of sensor noise models alone will not provide the required robustness at desired locations in the plant. A series of controller were developed using input uncertainty models that reflect a strong dependence of the controllers on accurate input signals to the system. As the input uncertainty level is increased in the control design model, there is a marked decrease in the closed-loop performance. Control designs for the flexible structure experiment are less sensitive to output uncertainty, which provides a very accurate description of the system when combined with the nominal model for control design. The output multiplicative control designs exhibit better performance both theoretically and experimentally as a function of uncertainty. The theoretical and experimental results indicate that structured uncertainty modeling plays a major role in the trade-off of performance requirements and robustness properties of synthesized control laws. In fact, it is interesting to note that the location and structure of the uncertainty in the problem formulation may be as important as the level of uncertainty.

The results presented in this paper indicate that a number of improvements can be made in modeling and identification methods for control of flexible structures to improved performance. Identification methods for robust control should produce both nominal models with additive noise and structured uncertainty models for incorporation into the control problem formulation. These identified models should then be used to improve the first principles model of the structure leading towards a more integrated framework in which structures and control design for flexible structures can be performed.

## Acknowledgment

The authors would like to thank Prof. A. Packard, Dr. K. Lim, Dr. P. Maghami, and Dr. E. Armstrong for many useful discussions.

## References

[1] G. J. Balas, "Robust control of flexible structures: Theory and experiments," Ph.D. dissertation, California Inst. Tech., Pasadena, 1989.
[2] G. J. Balas and J. C. Doyle, "Robust control of flexible modes in the controller crossover region," *AIAA J. Guidance, Contr. Dynamics*, vol. 17, no. 2, pp. 370–377, 1994.
[3] R. S. Smith, C. C. Chu, and J. L. Fanson, "The design of $\mathcal{H}_\infty$ controllers for an experimental noncollocated flexible structure problem," *IEEE Trans. Contr. Syst. Tech.*, vol. 2, no. 2, pp. 101–109, 1994.
[4] K. B. Lim, P. G. Maghami, and S. M. Joshi, "A comparison of controller designs for an experimental flexible structure," *IEEE Contr. Syst. Mag.*, May–June, 1992.
[5] J. Fanson, C. C. Chu, B. Luire, and R. Smith, "Damping and structural control of the JPL phase 0 testbed structure," *J. Intelligent Material Systems and Structures*, vol. 2, pp. 281–300, July 1991.
[6] D. W. Sparks and J. N. Juang, "Survey of experiments and experimental facilities for control of flexible structures," *AIAA J. Guidance, Contr. Dynamics*, vol. 15, no. 4, pp. 801–816, 1992.
[7] E. G. Collins, J. A. King, D. J. Phillips, and D. C. Hyland, "High performance, accelerometer-based control of the Mini-MAST structure," *AIAA J. Guidance, Contr. Dynamics*, vol. 15, no. 4, pp. 885–892, 1992.
[8] G. J. Balas and J. C. Doyle, "Identification and robust control for flexible structures," *IEEE Contr. Syst. Mag.*, vol. 10, no. 4, pp. 51–58, June, 1990.
[9] J. C. Doyle, "Analysis of feedback systems with structured uncertainties," in *IEE Proc.*, vol. 129, part D, no. 6, Nov. 1982, pp. 242–250.
[10] A. K. Packard, "What's new with $\mu$: Structured uncertainty in multivariable control," Ph.D. dissertation, Univ. California, Berkeley, 1988.
[11] A. K. Packard and J. Doyle, "The complex structured singular value," *Automatica*, vol. 29, no. 1, pp. 71–109, 1993.
[12] G. J. Balas, J. C. Doyle, K. Glover, A. K. Packard, and R. Smith, *$\mu$-Analysis and Synthesis Toolbox: User's Guide.* MUSYN Inc. and The Mathworks, 1990.
[13] J. C. Doyle, K. Glover, P. P. Khargonekar and B. A. Francis, "State-space solutions to standard $H_2$ and $H_\infty$ control problems," *IEEE Trans. Automat. Contr.*, vol. 34, no. 8, pp. 831–847, Aug. 1989.
[14] G. J. Balas, J. Reiner, and W. L. Garrard, "Design of a flight control system for a highly maneuverable aircraft using $\mu$ synthesis," in *Proc. AIAA Conf Guidance, Navigation, Contr.*, Monterey, CA, Aug., 1993.
[15] J. C. Doyle, K. Lenz, and A. K. Packard, "Design examples using $\mu$ synthesis: Space shuttle lateral axis FCS during reentry," in *Proc. IEEE Conf. Decis. Contr.*, Dec. 1986, pp. 2218–2223.
[16] A. K. Packard, J. C. Doyle, and G. J. Balas, "Linear, multivariable robust control with a $\mu$ perspective," *ASME J. Dynamics, Measurements and Contr.*, vol. 115, no. 2b, pp. 426–438, June 1993.

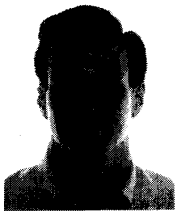

**Gary J. Balas** (S'89–M'89) received the B.S. and the M.S. degrees in civil and electrical engineering from the University of California, Irvine, and the Ph.D. degree in aeronautics from the California Institute of Technology in 1990.

Since 1990, Dr. Balas has been a faculty member in the Department of Aerospace Engineering and Mechanics at the University of Minnesota and currently holds the McKnight–Land Grant Professorship. He is a Co-organizer and Developer of the MUSYN Robust Control Short Course and the $\mu$-Analysis and Synthesis Toolbox used with MATLAB and is the President of MUSYN Inc. His current research interests include control of flexible structures, aircraft, model validation, and industrial applications of robust control methods.

**John C. Doyle** received the B.S. and the M.S. degrees in electrical engineering from the Massachusetts Institute of Technology, Cambridge, in 1977 and the Ph.D. degree in mathematics from the University of California, Berkeley, in 1984.

He is a Professor of Electrical Engineering at California Institute of Technology, Pasadena, and has been a consultant to Honeywell Systems and Research Center since 1976. His theoretical research interests include modeling and control of uncertain and nonlinear systems, matrix pertubation problems, operator methods, and $\mu$. His theoretical work has been applied throughout the space industry and is gaining acceptance in the process control industry. His current application interests include flexible structures, chemical process control, flight control, and control of unsteady fluid control and combustion. Additional academic interests include the impact of control or system design, the role of neoteny in personal and social evolution, modeling and control of acute and chronic human response to exercise, and feminist critical theory, especially in the philosophy of science.

Dr. Doyle is the recipient of the Hickernell Award, the Eckman Award, the IEEE Control Systems Society Centennial Outstanding Young Engineer Award, and the Bernard Friedman Award. He is an NSF Presidential Young Investigator, ONR Young Investigator, and has coauthored two Transactions Best Paper Award winners, one of which won the IEEE Baker Prize.